

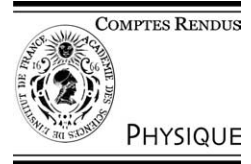


ELSEVIER

Available online at www.sciencedirect.com

SCIENCE @ DIRECT®

C. R. Physique 5 (2004) 483–493



Ultimate energy particles in the Universe/Particules d'énergies ultimes dans l'Univers

Energy determination of trans-EeV cosmic rays

Shigeru Yoshida

Department of Physics, Faculty of Science, Chiba University, Chiba 263-8522, Japan

Available online 8 May 2004

Presented by Pierre Encrenaz

Abstract

This article gives a summary of the primary energy estimation by observing ultra-high energy cosmic ray induced extensive air showers (down to the EeV energies – the energy range of the Japanese AGASA experiment). **To cite this article:** *S. Yoshida, C. R. Physique 5 (2004).*

© 2004 Académie des sciences. Published by Elsevier SAS. All rights reserved.

Résumé

Mesure de l'énergie des rayons cosmiques au-delà du EeV. Cet article est un résumé des méthodes utilisées pour la mesure de l'énergie des gerbes atmosphériques créées par les rayons cosmiques d'ultra-haute énergie (à partir de l'EeV, domaine de l'expérience japonaise AGASA). **Pour citer cet article :** *S. Yoshida, C. R. Physique 5 (2004).*

© 2004 Académie des sciences. Published by Elsevier SAS. All rights reserved.

Keywords: Lateral distribution function; Shower fluctuations; Atmospheric fluorescence; Energy spectrum; Rayleigh and Mie scattering

Mots-clés : Fonction de distribution latérale ; Fluctuations des gerbes ; Fluorescence atmosphérique ; Spectre d'énergie ; Diffusion Rayleigh et Mie

1. Introduction: overview of the detection techniques

The intensity of Ultra-High Energy Cosmic Rays (UHECR) is unfortunately painfully low: 1 event per km² sr and per century for particles with energies greater than 10²⁰ eV. Consequently their observation requires detection techniques with a huge acceptance which have always been challenging to build because of technological and economical difficulties.

The good news is, however, that an UHECR particle entering the atmosphere does not penetrate but collides with air molecules to initiate shower cascades ending up with billions of sub-particles before reaching ground surface. These sub-particles, which mainly consist of electrons, positrons and photons, form a disc of particles looking like a pancake with a radius increasing with energy, up to several kilometers. Therefore just sampling the particles inside the disk can be a reasonably good way to measure the UHECR properties. Air itself is a good target material and also a good calorimeter. The shower cascade in air initiated by cosmic rays is called Extensive Air Shower (EAS) which has been playing a key role in the detection of cosmic ray particles. There are two types of detection techniques available to measure the energy (as well as the arrival directions and mass composition) of the primary UHECR particles: the Ground Arrays and the Fluorescence Detectors.

The two methods are highly complementary: the ground array method measures the *lateral* development of EAS cascades. The dynamics to determine the behavior of the lateral spread of particle distributions in EAS is well understood and rather reliable, regardless of the mass of the primary cosmic rays, but some uncertainties remain due to our incomplete knowledge concerning the hadronic interactions and the multiple scattering of secondary electrons. The fluorescence method observes the

E-mail address: syoshida@hepburn.s.chiba-u.ac.jp (S. Yoshida).

longitudinal development of cascades. It is similar to the concept of calorimetric detectors in high energy physics, since the fluorescence light generated by the charged particles in the shower is proportional to the energy deposited in the atmosphere.

These two methods are complementary since they view different components of the EAS. The ground array observes the particles at ~ 1 km away from the EAS axis while the fluorescence method is sensitive to particle energy distributions very close to the shower axis, typically less than 100 m. Therefore, both methods have their own advantage and disadvantage as far as the energy estimation is concerned. In the following sections, we discuss how to deduce the primary energy and the possible sources of the systematic uncertainties.

2. The ground array method

2.1. Overview

The ground array experiments sample the charged secondary shower particles as they reach the ground. They determine the primary energy from the particle density, the arrival direction from the detector trigger times, and may infer the primary chemical composition from the ratio of the muon to electron component. The typical detection system is an array which consists of distributed surface detectors such as plastic scintillators across a large area to measure the density of charged particles – mainly electrons and positrons – reaching the detector. Each surface detector essentially measures the energy deposit of charged particles penetrating the detector. This can then be converted to a number of particles by normalizing it with the energy deposit of a muon. Another technique consists in deploying tanks filled with water. The particle density (electrons, muons and photons converted into electron–positron pairs) is estimated by the Čerenkov light they generate in the water. Both detectors aim at measuring the lateral distribution of particles in the EAS, i.e., the particle density distribution as a function of the distance from the shower core. This is the so called ‘lateral distribution function’ (LDF). The required area over which the particle counters are distributed is related to the rate of events initiated by UHECRs and the separation of the detectors is optimized to match the size of the footprint left by the EAS on the ground. Fig. 1 shows an example of event detected by the Akeno Giant Air Shower Array (AGASA) [1] whose detector separation is about 1 km. The particle density is estimated by measuring the intensity of scintillation light generated by the energy lost by the particles in the scintillators. The averaged energy loss is about 10 MeV for a plastic scintillator of 5 cm thickness which is 0.14 times the electron radiation length (37 g/cm^2).

The primary energy of an UHECR is proportional to the total number of particles in the EAS, which cannot be measured directly for obvious practical reasons. Instead the ground array method uses the fact that the number of particles at the maximum of an EAS cascade development is a good indicator of the primary energy. It has been found that

$$E = 1.4 \text{ GeV} \times N_{\text{max}}, \quad (1)$$

where N_{max} is the number of particles at the shower maximum. Because of this relation, the ground array method, essentially one layer sampling of EAS cascades, is reasonably good enough for estimation of primary energy of cosmic rays.

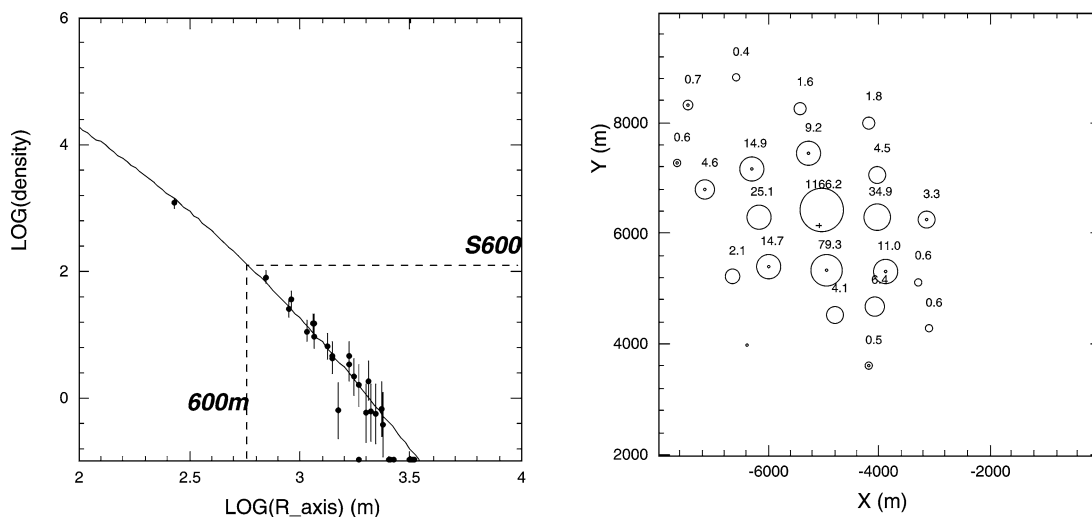


Fig. 1. A typical EAS event detected by the Akeno Giant Air Shower Array (AGASA). Left: lateral distribution of charged particles detected by AGASA. Right: map of the density distribution of the event. The surface of each circle is proportional to the particle density. A cross shows the estimated location of the shower core.

In practice, however, the energy determination based on Eq. (1) is not feasible because with this method one must always detect an EAS at its maximum. The atmospheric slant depth (total thickness of air seen by the shower) actually depends on the zenith angle at which an UHECR particle enters the atmosphere and the showers often reach the detection level well after their maximum in the cascade development. Moreover, the shower maximum fluctuates considerably from event to event because of the stochastic nature of the hadronic cascades along the shower axis. It is necessary to establish a method which is less sensitive to the absolute position of the shower maximum in an individual event. Also it should be noted that the method based on Eq. (1) to measure the primary energy would have technical difficulties since the estimation of N_{\max} must rely on the measurement of particle densities close to the core where, in most cases (giant arrays with wide detector separation), there are no particle counters to record the density.

These considerations led to a suggestion by Hillas that the fluctuations of the particle densities far from the core are reasonably small and hence the LDF at such distances (a few hundred meters to one kilometer) can be a good energy indicator [2]. Monte Carlo simulations have indeed shown that the density far from the core is quite stable, it is proportional to the primary energy and is only weakly dependent on the hadronic interaction process and on the primary composition of UHECR particles. This is due to the fact that shower particles far from the core are produced at an early stage of the shower cascading and scattered out by the well understood Coulomb interaction. The particle density 600 m from the shower core, $S(600)$, has been used to determine the primary energy as shown in Fig. 1. The conversion factor from $S(600)$ to E depends on the type of detectors and on the altitude of the site where the array is located. For the AGASA using plastic scintillators of 5 cm thickness, we find

$$E = 2.03 \times 10^{17} \left(\frac{S(600)}{1 \text{ m}^{-2}} \right) \text{ eV}, \quad (2)$$

by using the COSMOS shower simulation program. For the next-generation experiment, the Auger observatory [3] for which currently water Čerenkov detectors are deployed, this empirical formula becomes

$$E = 5.25 \times 10^{17} \left(\frac{S(600)}{1 \text{ m}^{-2}} \right) \text{ eV} \quad (3)$$

if the detectors were located at sea level. This difference mainly arises from the fact that signals in water Čerenkov detectors mainly come from muons that penetrate the detector while the plastic scintillator is more sensitive to low energy electrons and photons.

2.2. The analysis procedure to estimate the primary energy

In the previous section, we explained the basic ideas on how to go from the measured density at, say, 600 m from the shower core to the primary energy. Recently more modern Monte Carlo simulations including full detector simulations (e.g., the response of the plastic scintillators to electrons and photons) have been carried out to confirm that Eq. (2) represents fairly well the reality [4]. Fig. 2 shows the relation obtained by the ARES Monte Carlo simulation [5] package with the AGASA full detector simulation. The hadronic interactions are assumed to follow the QGSJET model [6], which includes minijet production in hadronic interactions and has been considered to be the best suited to reconstruct the EAS parameters at low energies and to extrapolate them to the UHE region. A fairly good agreement is found between the conversion factor given by Eq. (2) and the recent estimations. The difference has been found to be about 20% at 10^{20} eV.

In the energy conversion relation, $S(600)$ is the density for vertical air showers at the Akeno altitude (900 m above sea level). Showers initiated by UHECR particles entering atmosphere at a zenith angle θ will have smaller densities $S_{\theta}(600)$ since the atmospheric slant depth for those showers is larger. This attenuation effect of the density has been measured by ‘equi-intensity cuts’ on the integral $S_{\theta}(600)$ spectra, based on the assumption that the rate of showers above certain primary energy does not change with atmospheric depth. Fig. 3 shows the measured attenuation curves of $S(600)$ for five different intensities (hence different primary energies). The measurements, in case of AGASA, can be approximated by an exponential function [7]:

$$S_{\theta}(600) = S(600) \exp \left[-\frac{X_0}{500} (\sec \theta - 1) - \frac{X_0}{594} (\sec \theta - 1)^2 \right], \quad (4)$$

where X_0 is 920 g cm^{-2} , the atmospheric depth at Akeno.

2.3. Energy resolution and systematic errors

In the AGASA experiment, the resolution on the energy is directly related to that on $S(600)$. The accuracy on $S(600)$ depends on the fluctuations in the shower development, and on the resolution of the scintillation detector, on statistical fluctuations of particles hitting each surface detector. Fluctuations on $S(600)$ due to the cascade development have been studied in detail by

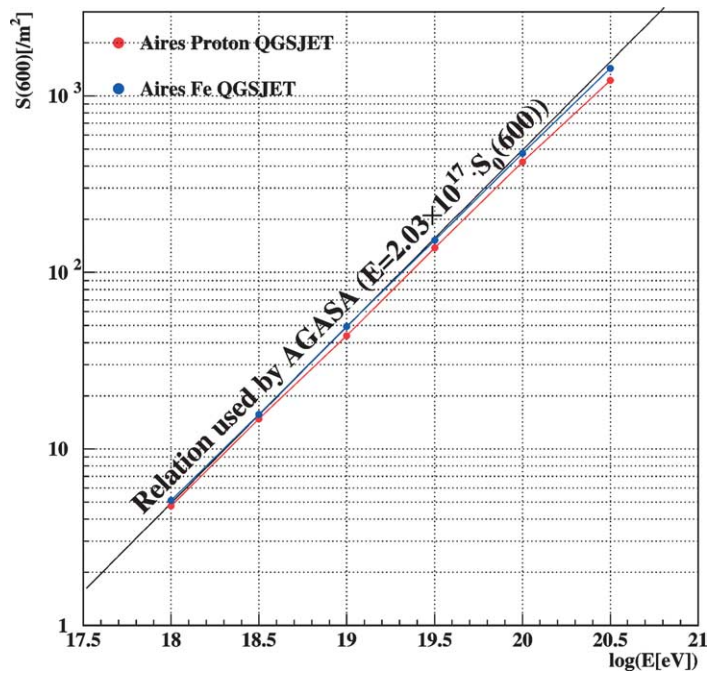


Fig. 2. Relation between $S(600)$ and primary energy estimated based on the QGSJET model.

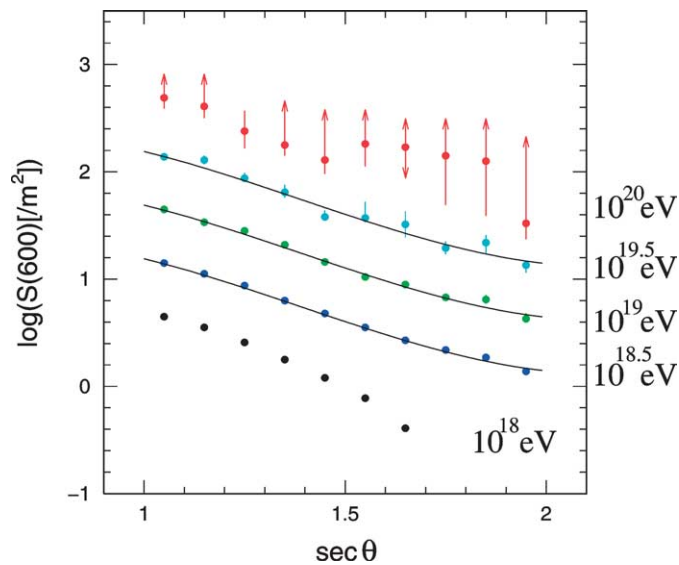


Fig. 3. Variation of $S(600)$ with the zenith angle obtained by using the method of ‘equi-intensity cuts’. The solid curves correspond to the most probable attenuation curve represented by Eq. (4) derived from integral $S(600)$ spectra.

Monte Carlo methods. Its dependence on the shower zenith angle is $\sim 15\%$ for vertical showers and $\sim 40\%$ at $\theta = 45^\circ$ for EAS with energies of 10^{18} eV. The FWHM (full width at half maximum) of the scintillation detector yield is $\sim 80\%$ for a vertically incident particle on the scintillator. This means our detector resolution is $\sim 25\%$ in case of 10 particles crossing the detector. The simulation including all these fluctuations gives the overall energy resolution $\pm 30\%$ for events with $E \geq 10^{19}$ eV and $\sec \theta \leq 1.4$ [8].

Systematic energy uncertainties arise from systematic errors in the calibration of each detector, but also uncertainties in the shape of the LDF, in the attenuation curve of $S(600)$, and in the energy conversion from the $S(600)$ parameter. Let us consider each contribution.

- The uncertainty in the calibration of each detector is mainly caused by variations of the gain and linearity response of the amplification system. The gain has been determined in every run by monitoring the pulse spectrum of vertical muons. The detector linearity can also be monitored by the spectral slope of the pulse height distribution. The result is that the overall uncertainty due to the detector calibration is $\sim 5\%$ for recording 100 particles per detector.
- The probable systematic errors due to limited accuracy in the determination of η in the LDF have been discussed in the literature. The LDF obtained by the AGASA measurement is given by [7]:

$$\rho(R) = C \left(\frac{R}{R_M} \right)^{-1.2} \left(1 + \frac{R}{R_M} \right)^{-(\eta-1.2)} \left[1.0 + \left(\frac{R}{1000} \right)^2 \right]^{-0.6}, \quad (5)$$

$$\eta = 3.97 - 1.79(\sec \theta - 1).$$

Here R_M is the Molière radius (91.6 m at Akeno), calculated at two radiation lengths above the central laboratory at the Akeno Observatory. C is a normalization factor and η is a parameter which determines the slope of the LDF at $R \geq R_M$. The processes to search for the arrival direction and the core location are repeated several times to give the most probable values. Then the particle density at 600 m from the core, $S_\theta(600)$, is calculated using the best estimated core position and the LDF. The systematic deviation in $S(600)$ due to the uncertainty in the LDF was found to be $\sim \pm 5\%$ for almost vertical showers, $\sim \pm 10\%$ for showers with $\sec \theta = 1.4$, and $\sim \pm 20\%$ for showers with $\sec \theta = 1.6$.

- The limited accuracy of the attenuation curve represented by Eq. (4) also generates uncertainties in the estimated value of $S(600)$ after conversion from $S_\theta(600)$. The conservative estimation is $\sim 20\%$ for events with $\sec \theta = 1.4$.
- It is more difficult to evaluate the uncertainties in the energy conversion relation given by Eq. (2) because it relies on the shower cascade simulations with incomplete knowledge of the hadronic interaction at ultra high energies. The insensitivity of the $S(600)$ to the interaction model does not totally exempt its model dependence. But there are some clues. The recent Fly's Eye, AGASA and Yakutsk data favor models with a dissipation of energy faster than in scaling models and limit the allowed variations of hadronic interaction models. The AIRES Monte Carlo simulation using the QGSJET and SIBYLL models both of which exhibit a quicker dissipation has shown that the systematic difference due to the model dependence is likely to be less than 40% for 10^{20} eV cosmic rays no matter if they are protons or irons. There is a difference between QGSJET [6] and SIBYLL [9] or between proton and iron showers but it should be noted that any combination assigns a higher energy than that estimated by Eq. (2) based on the COSMOS program [10]. We should keep this trend in mind in interpreting the observed data. The less significant systematic error also arises from the dependence on the lateral distribution of electrons (LDE) used in the simulation, where the analytical LDE function is applied to each electron after its generation in the shower development. Details of the LDE and the value for the radiation length at the observation level differ in various calculations, but the resultant systematic errors due to the LDE may not be significant, since electromagnetic cascades may be scalable to the highest energy. More experimental estimations of the systematics have been made by comparison of the AGASA relation, Eq. (2), to those by the Yakutsk group where they measure energies carried by electromagnetic components and muons (neutrinos), not only on the surface and underground, but also in the atmosphere by detecting the Čerenkov light emitted by the EAS. It is found that the conversion relation determined from the Yakutsk experiment is 15% larger than the relation by Eq. (2), much less than the conservative values obtained by simulation with the QGSJET and the SIBYLL models.

3. The air fluorescence method

The air fluorescence technique consists in detecting the EAS by the measurement of the ultraviolet fluorescence of molecular nitrogen generated by the air shower particles. Unlike Čerenkov radiation, this fluorescence is isotropic and hence it can be seen from any angle by appropriate detectors. This fluorescence yields about four photons per meter of ionizing particle trajectory along the EAS axis, which are collected by a light collector system such as reflection mirrors and recorded with a ultraviolet-sensitive camera like a mosaic of photomultiplier tubes. As an air shower cascade develops, emitted ultraviolet photons, passing through the field of view of the optical detectors, generate time-dependent signals. This defines a moving track through the atmosphere, from which one can reconstruct the longitudinal shower profile. The integral of the reconstructed profile is directly proportional to the primary energy of a UHECR initiating the EAS. This method is essentially calorimetric. It consists in measuring the total energy deposit in the atmosphere by the charged particles. It does not need a complex Monte Carlo simulation to determine the energy scale, which would be required in the ground array technique. The identification of the

primary particle is made by examining the shape of the longitudinal profile of the shower. The atmospheric depth of the shower maximum (X_{\max}) is a good parameter for the identification. This technique has a great potential to discriminate gamma rays and neutrinos from cosmic ray hadrons, which is an important experimental signature in the search for the origin of UHECRs.

3.1. Overview

General features of the fluorescence method using an optical detector which consists of a system of mirrors and light collecting opto-electronic devices (phototubes, pixels) can be easily obtained by the following arguments [11]: a signal in a phototube is significant for the reconstruction of an event only if it collects more air fluorescence light emitted by the shower track than the fluctuations of the night sky background light during its integration time t_{gate} . Part of the fluorescence light is scattered out on its way to the detector due to collisions with the air molecules (the Rayleigh scattering) or with dust, pollution, fog, and clouds (the Mie scattering). The expected air fluorescence signal is thus given by

$$N_{\text{ph}} = \frac{A_{\text{mir}} N_e Q}{4\pi r_p^2} \exp\left(\frac{-r_p}{r_0}\right) e_{\text{eff}} r_p \Delta\theta, \quad (6)$$

where r_p is distance to a fluorescence emission point along the shower axis from the detector, A_{mir} is the area of the mirror in the detector, N_e is the number of electrons in the shower cascade viewed by a given phototube, r_0 is the extinction length of light due to the atmospheric scattering, e_{eff} is the fluorescence light yield from an electron (in photons per meter), $\Delta\theta$ is the phototube pixel size (field of view) and Q is the quantum efficiency of the phototube. The background light is given by

$$N_{\text{BG}} = n_{\text{NB}} t_{\text{gate}} A_{\text{mir}} Q (\Delta\theta)^2, \quad (7)$$

where n_{NB} is the night sky photon intensity and t_{gate} is the gate time for collecting the signal. Then the signal to noise ratio n_{th} gives the threshold shower electron size for triggering a channel as a function of r_p as follows:

$$N_{e,\text{th}} = n_{\text{th}} 4\pi r_p \exp\left(\frac{r_p}{r_0}\right) e_{\text{eff}}^{-1} \sqrt{\frac{n_{\text{NB}} t_{\text{gate}}}{A_{\text{mir}} Q}}. \quad (8)$$

When $r_p \gg r_0$, which is the most frequent case, this equation can be written as

$$\begin{aligned} \log N_{e,\text{th}} = & 7.54 + \left(\frac{r_0}{8 \text{ km}}\right)^{-4/5} 8.23 \times 10^{-2} \left(\frac{r_p}{1 \text{ km}}\right) \\ & + \log \left[n_{\text{th}} \left(\frac{r_0}{8 \text{ km}}\right) \left(\frac{e_{\text{eff}}}{4 \text{ m}^{-1}}\right)^{-1} \left(\frac{R_{\text{mir}}}{1 \text{ m}}\right)^{-1} \sqrt{\left(\frac{n_{\text{NB}}}{10^6 \text{ m}^{-2} \text{ s r}^{-1} \mu\text{s}^{-1}}\right) \left(\frac{t_{\text{gate}}}{5 \mu\text{s}}\right)} \right], \end{aligned} \quad (9)$$

where R_{mir} is the radius of the mirror and Q is assumed to be 30%.

The atmospheric slant width over which the shower cascade contains more electrons than this threshold size $N_{e,\text{th}}$ can be numerically obtained as the following expression:

$$\begin{aligned} X_t^{100\%} & \equiv X_t(N_e \geq N_{e,\text{th}}) = 100(-\eta^2 - 8\eta + 2) [\text{g/cm}^2], \\ \eta & = \log(N_{e,\text{th}}) - \log\left(\frac{E}{1 \text{ GeV}}\right). \end{aligned} \quad (10)$$

Using Eq. (9), η can be written as a function of r_p and thus $X_t^{100\%}$ is a function of E and r_p . To trigger showers with a given geometry and energy, $X_t^{100\%} \geq 0$ must be required, which leads to a maximum shower distance at which the optical detector will trigger:

$$r_p^{\text{max}} = 12.15 \left(\frac{r_0}{8 \text{ km}}\right)^{4/5} f [\text{km}], \quad (11)$$

where

$$f = 2.7 + \log\left(\frac{E}{10^{19} \text{ eV}}\right) - \log \left[n_{\text{th}} \left(\frac{r_0}{8 \text{ km}}\right) \left(\frac{e_{\text{eff}}}{4 \text{ m}^{-1}}\right)^{-1} \left(\frac{R_{\text{mir}}}{1 \text{ m}}\right)^{-1} \sqrt{\left(\frac{n_{\text{NB}}}{10^6 \text{ m}^{-2} \text{ s r}^{-1} \mu\text{s}^{-1}}\right) \left(\frac{t_{\text{gate}}}{5 \mu\text{s}}\right)} \right]. \quad (12)$$

At 10^{19} eV with $n_{\text{th}} = 2$ (2σ deviation) then $r_p^{\text{max}} \sim 29$ km for the detectors operating in a desert atmosphere.

From the arguments above, general consequences on this detection method can be obtained. First the typical distance scale to observable EAS from the optical detector is ~ 30 – 40 km as expressed in Eqs. (11) and (12) which depends only weakly on

the detector parameters such as the mirror area and the pixel size of a phototube. This is because most of the light produced by the shower is scattered out by the Rayleigh and Mie processes and is therefore significantly reduced. The exponential term in Eq. (6) dominates in the overall contributions. This consideration leads to the second consequence: the atmospheric monitoring to measure the extinction length r_0 is crucial. The primary energy of an UHECR particle is approximately proportional to the signal from the initiated air shower and Eq. (6) shows that the uncertainty on the energy determination is related to the extinction length as

$$\frac{\Delta E}{E} \simeq \frac{r_p}{r_0} \frac{\Delta r_0}{r_0}. \tag{13}$$

This means that we must determine r_0 with an accuracy of 5% to estimate the energy of events at ~ 30 km from the detector with a systematic error of 10%. This is challenging, but not impossible because contribution of the Rayleigh scattering dominates over the Mie scattering process in the fluorescence light propagation and effects of the Rayleigh scattering can be accurately predicted because it is a rather simple electromagnetic process. Lots of methods to measure the extinction length have been proposed and performed [12,13]. They are based on measurements of laser and ‘flasher’ shots fired through the detector aperture [14]. Two approaches are possible. One uses selected geometries to deconvolve the effects of the Mie scattering and measure the transmission rate. The second fits an aerosol model to the observed data to determine the model parameters. These parameters include a horizontal attenuation length, an aerosol scale height, and a scattering dependence or phase function. More technical details can be found in [14].

One more consequence from these arguments is that the estimation of the primary energy relies on the geometrical reconstruction of observed events because the intensity of the signal strongly depends on r_p as expressed in Eq. (6). An ultra high energy EAS can only produce very weak signals if it is very far from the detector, in contrast to the ground array technique where the higher energy event has a larger and denser footprint on the array surface. Therefore the accuracy of the geometrical reconstruction is important not only for studies of the arrival directions, but also for a reliable energy determination. Fortunately, the achievable resolution of the geometrical reconstruction is good enough since the event geometry can be deduced by not only the geometrical information of the recorded event track in the camera but also by its timing information. In other words, the signal profile in intensity and time strongly depends on the detector-shower axis geometry. Fig. 4 illustrates how the event geometry determines the signal profile. Provided the data recording system is capable of sampling the signal from the shower with constant frequency, the longitudinal direction α_j of the light spot seen by the station i along the shower track is related to a given event geometry and relative timing of the j th sampling as follows.

$$\alpha_j = \pi - \psi_i - 2 \tan^{-1} \left[\frac{c}{R_p^i} \left(t_j - t_0 - \frac{\mathbf{n}_s \cdot \mathbf{r}_i}{c} \right) \right], \tag{14}$$

where R_p^i is the impact parameter from station i , \mathbf{n}_s is direction of the shower axis, \mathbf{r}_i is the vector from the station to the core position, and t_0 the absolute origin of the timing. Consequently the signal profile at every sampling time, i.e., how the light spot crosses the phototube, is a function of the geometrical parameters via Eq. (14). Good geometrical resolution is hence obtained by minimizing the χ^2 built by comparison of the prediction of the signal profile by Monte Carlo simulation with the recorded profile at every sampling frequency. Another key to a good resolution is to achieve a stereoscopic view of the shower profile. This is made possible by having two or more stations of optical detectors with 10–40 km separation. Then one has a model independent way of checking the resolution of the energy and depth of shower maximum (X_{\max}). This way, the energy and X_{\max} are measured independently by each station. Comparing them with the stereoscopic reconstruction improves strongly the

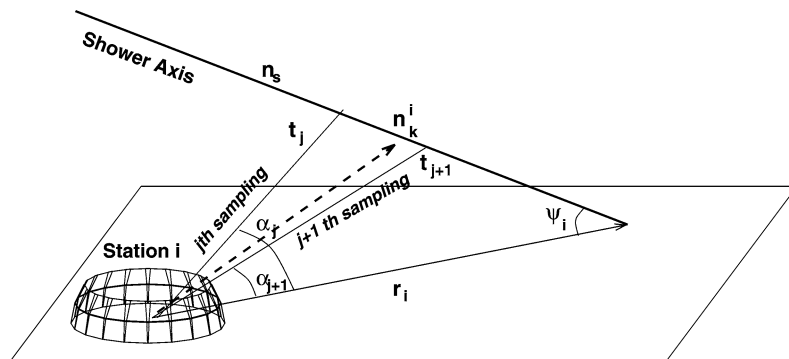


Fig. 4. Geometrical relations between the event track and the optical detectors.

resolution without relying on a complex Monte Carlo simulation. In today's fluorescence detectors, the stereoscopic observation capability is seen as a mandatory function.

3.2. Calorimetric energy measurement

The calorimetric energy measurement is the main advantage of the air fluorescence method. The total energy deposit in the atmosphere is

$$E^{\text{deposit}} = \int dX N_e(X) \alpha(\varepsilon, S(X)), \quad (15)$$

where $N_e(X)$ is number of electrons in the shower as a function of depth in the atmosphere and where X is measured in unit of g/cm^2 . The longitudinal shower profile $N_e(X)$ is analytically well described by the Gaisser–Hillas formula:

$$N_e(X, X_{\text{max}}, X_1, N_{\text{max}}) = N_{\text{max}} \left(\frac{X - X_1}{X_{\text{max}} - X_1} \right)^{(X_{\text{max}} - X_1)/\lambda} \exp\left(\frac{X_{\text{max}} - X}{\lambda} \right). \quad (16)$$

Here X_{max} is the shower maximum, X_1 is atmospheric depth at the first interaction point of the shower, and λ is the attenuation length which is approximately $70 \text{ g}/\text{cm}^2$. The parameter α in Eq. (15) is the energy loss per charged particle in air via ionization, which is given by [15]

$$\alpha(\varepsilon, S(X)) = \int_{\varepsilon} dE_e \frac{dE_e}{dX} n_e(E_e, S), \quad (17)$$

where n_e is the differential energy spectrum of electrons, dE_e/dX is the ionization loss rate for an electron as a function of its kinematic energy E_e and ε is the threshold energy in this integral, which is presumably zero in real events. Finally $S(X)$ is the 'age' parameter, which is defined as

$$S(X) = \frac{3(X - X_1)}{(X - X_1) + 2(X_{\text{max}} - X_1)}. \quad (18)$$

The number of the fluorescence photons is given by

$$N_{\gamma}^{\text{fl}} = \int dX N_e(X) \frac{dL}{dX} \int_{\varepsilon} dE_e \frac{dY^{\text{fl}}}{dL} n_e(E_e, S), \quad (19)$$

where dY^{fl}/dL is the air fluorescence yield in photons per unit length which can be formalized as [16]

$$\frac{dY^{\text{fl}}}{dL} = \kappa^{-1} \frac{dE_e}{dX} f(\rho, T) = \kappa^{-1} \frac{dE_e}{dX} \sum_i \rho \frac{A_i}{1 + B_i \rho \sqrt{T}}. \quad (20)$$

Here ρ is the air density [g/cm^3], T is the temperature [K], and A_i and B_i are the constant coefficients to take into account its dependence on the wavelength. The normalization coefficient κ is chosen so that

$$\kappa = \left(\frac{dE_e}{dX} \right)_{[E_e=1.4 \text{ MeV}]} \simeq 1.668 \text{ MeV}/\text{g}/\text{cm}^2 \quad (21)$$

for practical reasons. The fact that the fluorescence yield is proportional to dE_e/dX as expressed in Eq. (20) guarantees that the fluorescence detectors can measure E^{deposit} in a calorimetric way. Comparing Eqs. (15), and (17) with Eq. (19), we get

$$\frac{dE^{\text{deposit}}}{dX} = \frac{dN_{\gamma}^{\text{fl}}}{dL} \kappa f^{-1}(\rho, T) \quad (22)$$

which is independent of $\alpha(\varepsilon, S)$ and directly shows the calorimetric energy measurement.

It should be remarked, however, that it is necessary to calculate $\alpha(\varepsilon, S)$ to obtain the longitudinal shower profile $N_e(X)$ from the measured number of fluorescence photons N_{γ}^{fl} . From Eqs. (15), (19) and (20), we see that the reconstructed shower profile N_e^{rec} is given by

$$N_e^{\text{rec}}(X, \varepsilon) = \frac{dN_{\gamma}^{\text{fl}}}{dL} \kappa f^{-1}(\rho, T) \alpha^{-1}(\varepsilon, S). \quad (23)$$

Calculation of $\alpha(\varepsilon, S)$ relies on Monte Carlo simulations, and for technical reasons the threshold energy ε cannot be set at 0 MeV. The value $\varepsilon = 0.1 \text{ MeV}$ has been often used in the actual simulations. The reconstructed shower profile $N_e^{\text{rec}}(X)$

is a function of ε , and therefore depends on simulation and (weakly) on the mass of the primary particles. However X_{\max} (a parameter of paramount importance to identify the primary UHECR particles) is mainly determined by $\alpha(\varepsilon, S)$ at around $S = 1$. Its value is then very stable and almost independent of the primary mass and energy. The current value is $\alpha(0.1 \text{ MeV}, 1) \simeq 2.19 \text{ MeV/g/cm}^2$ [15]. Hence there are no major systematic uncertainties coming from the simulation in the evaluation of X_{\max} . Note that Eq. (23) also gives

$$E^{\text{deposit}} = \int dX N_e^{\text{rec}}(X, \varepsilon) \alpha(\varepsilon, S(X)) = \int dX N_e(X) \alpha(0, S(X)) \quad (24)$$

indicating again that the deposited energy measurement is independent of ε and free from assumptions in the shower Monte Carlo simulations.

For most of the observed events, however, the primary energy measurement partly relies on the reconstructed shower profile $N_e^{\text{rec}}(X, \varepsilon)$ derived by the simulation-dependent procedure via $\alpha(\varepsilon, S)$ because only a part of the longitudinal profile is usually within the field of view of the optical detectors and we must extrapolate the invisible part of the profile by the Gaisser–Hillas formula with X_{\max} and X_1 determined by the detected part of the profile. The detected signal intensity per unit length in number of photoelectrons per meter is related to $N_e^{\text{rec}}(X, \varepsilon)$ as follows:

$$\frac{dN_{\text{pe}}}{dL} = \frac{N_e^{\text{rec}}(X, \varepsilon)}{4\pi r_p^2} \kappa^{-1} f(\rho, T) \alpha(\varepsilon, S) A_{\text{mir}} \int d\lambda T_M(\lambda) \exp\left[-\frac{\Delta X_{\text{det}}}{\lambda_R} \left(\frac{400 \text{ nm}}{\lambda}\right)^4\right] f_{\text{fl}}(\lambda) \varepsilon_{\text{det}}(\lambda), \quad (25)$$

where ΔX_{det} is the atmospheric slant depth between the location of a mirror and the light-emission point along the shower axis, $f_{\text{fl}}(\lambda)$ is fluorescence wavelength spectrum, T_M is the light propagation transmission factor, taking into account the Mie scattering, λ_R is the extinction length of the Rayleigh scattering and $\varepsilon_{\text{det}}(\lambda)$ is the overall detection efficiency determined by the quantum efficiency of the phototube, transmission factor of the optical filters, reflectivity of the mirrors, dead space of a camera and so on. This equation is essentially equivalent to Eq. (6) but takes into account the dependence on the wavelength. Then the reconstructed $N_e^{\text{rec}}(X, \varepsilon)$ gives E^{deposit} by the energy integral of Eq. (15). It should be noted that this integral is mostly determined by the shower profile at around X_{\max} . Therefore, as long as the profile around the shower maximum is directly viewed by the detectors, the dominant contribution in the energy integral is given by the calorimetric measurement as expressed by Eq. (22) and the resultant energy deposit measurement is almost independent of $\alpha(\varepsilon, S)$.

It is true that E^{deposit} is calorimetrically measured, but the primary energy of an UHECR particle E would not be same as E^{deposit} because a part of the primary energy is taken by neutrinos, high energy muons and nuclear excitation. Even for γ -ray induced showers there is a tiny ‘missing energy’ because of the photo-nuclear interactions and the $\mu^+\mu^-$ pair production. The missing energy for γ -ray induced showers is only $\sim 1\%$ of the primary energy while that of hadronic showers is not negligible and some corrections are necessary. However, the correction factor decreases with increasing primary energy because charged pions produced in more energetic showers are more likely to interact than decay into muons and neutrinos. The simulation study [15] using CORSIKA [17] shows

$$\frac{E^{\text{deposit}}}{E} = 0.959 - 0.082 \left(\frac{E^{\text{deposit}}}{10^{18} \text{ eV}} \right)^{-0.15}. \quad (26)$$

This factor depends on the primary mass and there is about 5% difference between proton and iron-induced showers. The above function is an average of both.

3.3. Systematics errors

Let us summarize the sources of systematic uncertainties in the energy estimation.

- *Uncertainties in the PMT quantum efficiency, the PMT/preamp gain, and the mirror reflectivity*

The absolute gain and sensitivity of the detector must be calibrated and monitored. In the ground array method, signals from local muons passing through the particle counter are a good reference for the absolute calibration. It would be more difficult in the case of air fluorescence detectors, however, because there is no absolute light candle in nature. The standard procedure is to compare the signals produced by stable light sources such as UV LEDs, xenon flashers, and YAP pulsars equipping the optical detectors to those processed in the absolute calibration of the phototubes and electronics. Holding the overall uncertainty below 10% is the current reasonable goal for the calibration.

- *Uncertainty in the fluorescence yield*

Measurement of the energy deposit by the EAS relies on the fluorescence yield as expressed in Eq. (22). The yield has been well measured in a laboratory experiment [16]. However, the fluorescence yield for low energy electrons (below 1 MeV) is not quite understood, and the uncertainty is estimated at $\sim 10\%$.

- *Missing Energy*

As already described, the energy carried away by neutrinos and high energy muons in air shower cascades cannot be directly measured and must be estimated by Monte Carlo simulations. The correction factor depends on primary mass and there would be a 5% difference between proton and iron-induced showers [15]. This results in an unresolved systematic uncertainty in the primary energy estimation.

- *Atmospheric extinction*

Measurement of the atmospheric extinction length determines the dominant conversion factor from the number of photoelectrons recorded by the detector to the number of fluorescence photons radiated by the shower. As already noted, this may be the largest correction in the energy determination. The current goal is to keep the accuracy on the determination of the extinction length at the 10% level.

4. Reconstruction of the energy spectrum

The energy spectrum of UHECRs is a key clue for the understanding of the origin of UHE particle production. In order to reconstruct the spectrum, it is not only necessary to determine the energy of an individual event but also to calculate the detection efficiency, i.e., the *aperture* of the detector. The number of events per energy decade, $dN/d\log E$, which is directly measurable, is related to the differential flux $J(E) = dF/dE$:

$$\frac{dN}{d\log E} = T \frac{\ln 10}{\Delta \log E} \int d\Omega \int_{\log E - 0.5\Delta \log E}^{\log E + 0.5\Delta \log E} d\log \varepsilon J(\varepsilon) \varepsilon A(\log \varepsilon, \Omega). \quad (27)$$

Here T is the observation time, Ω the solid angle, A the aperture as a function of the solid angle and energy. The bin size $\Delta \log E$ being narrow enough, the log-differential flux $dF/d\log E$ is approximately given by:

$$\begin{aligned} \frac{dF}{d\log E} &\simeq \frac{dN}{d\log E} \Delta \log E \left(T \int d\Omega \int_{\log E - 0.5\Delta \log E}^{\log E + 0.5\Delta \log E} d\log \varepsilon A(\log \varepsilon, \Omega) \right)^{-1} \\ &\simeq \Delta N \left(T \int d\Omega \int_{\log E - 0.5\Delta \log E}^{\log E + 0.5\Delta \log E} d\log \varepsilon A(\log \varepsilon, \Omega) \right)^{-1}. \end{aligned} \quad (28)$$

As indicated in the equations above, the aperture $A(\log E, \omega)$ is essential in the flux estimation. Generally one must rely on proper Monte Carlo simulations to determine the aperture, which is always a source of systematic uncertainties. The efficiencies of the experimental trigger, the detector performance, and the detector dead time determine this factor and a careful comparison between the Monte Carlo predictions and observables is necessary for a reliable aperture calculation. This is a critical aspect of the fluorescence technique: the aperture increases with energy since the higher energy events produce enough light to be detected at large distances from the detector, as indicated in Eqs. (11) and (12). It also strongly depends on the atmospheric extinction length [represented as r_0 in Eq. (11)] and an accurate understanding of this parameter is also required.

The aperture estimation is much simpler for a ground array. The total aperture depends mainly on the array geometry. For events with energies well above the triggering threshold, the aperture becomes independent of energy and is determined by the surface of the array and the solid angle which, for practical reasons, the incident directions are limited to by the detection technique. Under stable conditions, no Monte Carlo simulation is needed for this purpose.

It should be remarked, however, that the reconstructed energy is *NOT* the true energy in all cases, because of the limited energy resolution. This affects the shape of the energy spectrum. This is an important point in both the fluorescence and the ground array techniques since we measure a steeply falling cosmic ray spectrum. For the energy resolution function $G(E_{\text{true}}, E_{\text{estimate}})$, Eq. (27) is rewritten as

$$\frac{dN}{d\log E} = T \frac{\ln 10}{\Delta \log E} \int d\Omega \int_{\log E - 0.5\Delta \log E}^{\log E + 0.5\Delta \log E} d\log \varepsilon \int d\varepsilon_{\text{true}} J(\varepsilon_{\text{true}}) \varepsilon_{\text{true}} A(\log \varepsilon_{\text{true}}, \Omega) G(\varepsilon_{\text{true}}, \varepsilon). \quad (29)$$

If the aperture A is independent of the energy, and if the energy resolution function G is Gaussian, one can deconvolute analytically J from the integration in this equation, but this is not always the case. The energy resolution function is usually determined by Monte Carlo simulation, but its deconvolution is a rather complicated and sometimes even tricky task. One method from the Akeno group has been to use Monte Carlo events and determine the aperture so that the output energy

spectrum reproduces the input E^{-3} spectrum. It works if the true spectrum is not very different from the assumed E^{-3} shape but this assumption makes it difficult to control the resultant systematic uncertainty. Another approach is to try various input spectra with $E^{-\gamma}$ shapes to fit the experimental data and estimate the ‘true’ power index γ . However, this method also requires an assumption, namely that the true spectrum follows a power law. More sophisticated methods which allow unfolding the spectrum without any assumption has been proposed. An example is the ‘regularized’ unfolding method [18] which consists in finding some base functions and represent any input spectrum by their linear combinations. It requires heavy CPU power but recent progress in improving the computing power has just started to make the bias-free unfolding possible. The next generation of UHECR experiments should be able to address this issue.

References

- [1] <http://www-akeno.icrr.u-tokyo.ac.jp/AGASA/>.
- [2] A.M. Hillas, et al., in: Proceedings of the 12th International Cosmic Ray Conference, vol. 3, Hobert, 1971, p. 1001.
- [3] <http://www.auger.org/>.
- [4] N. Sakaki, et al., in: Proceedings of the 26th International Cosmic Ray Conference, vol. 1, Humburg, 2001, p. 329.
- [5] <http://www.fisica.unlp.edu.ar/auger/aires/>.
- [6] N.N. Kalmykov, S.S. Ostapchenko, Phys. At. Nucl. 56 (1993) 346.
- [7] S. Yoshida, et al., J. Phys. G 20 (1994) 651.
- [8] S. Yoshida, et al., Astropart. Phys. 3 (1995) 105.
- [9] R.S. Fletcher, et al., Phys. Rev. D 50 (1994) 5710.
- [10] K. Kasahara, S. Torii, T. Yuda, in: Proceedings of the 16th International Cosmic Ray Conference, vol. 13, Kyoto, 1979, p. 70.
- [11] S. Yoshida, et al., Astrophys. J. 479 (1997) 547.
- [12] R. Cray, et al., Atmospheric monitoring via measurements of scattered light at the high resolution fly’s eye, in: D. Kieda, M. Salamon, B. Dingus (Eds.), Proceeding of the 26th ICRC, vol. 5, USA, August 17–25, 1999, University of Utah, Salt Lake City, 1999, p. 353.
- [13] M. Chikawa, et al., Atmospheric Monitoring for the telescope array project, in: D. Kieda, M. Salamon, B. Dingus (Eds.), Proceeding of the 26th ICRC, vol. 5, USA, August 17–25, 1999, University of Utah, Salt Lake City, 1999, p. 404.
- [14] L. Wiencke, et al., Nucl. Instr. Methods A 428 (1999) 593;
L. Wiencke, et al., in: R. Huffman, K. Dymond (Eds.), Ultraviolet Atmospheric and Space Remote Sensing: Methods and Instrumentation, in: Proc. SPIE, vol. 3818, 1999, p. 59.
- [15] C. Song, et al., Astropart. Phys. 14 (2000) 7.
- [16] F. Kakimoto, et al., Nucl. Instr. Methods A 372 (1996) 527.
- [17] D. Heck, et al., CORSIKA: A Monte-Carlo code to simulate extensive air showers, Report FZKA 6019, Forschungszentrum Karlsruhe, 1998.
- [18] CERN 8th school of computing, CERN Yellow Report 85-09, <http://cdsweb.cern.ch/>.